Volume 10
Number 6
June 2025
Pages 427–496

MSDE

Molecular Systems Design & Engineering

rsc.li/molecular-engineering

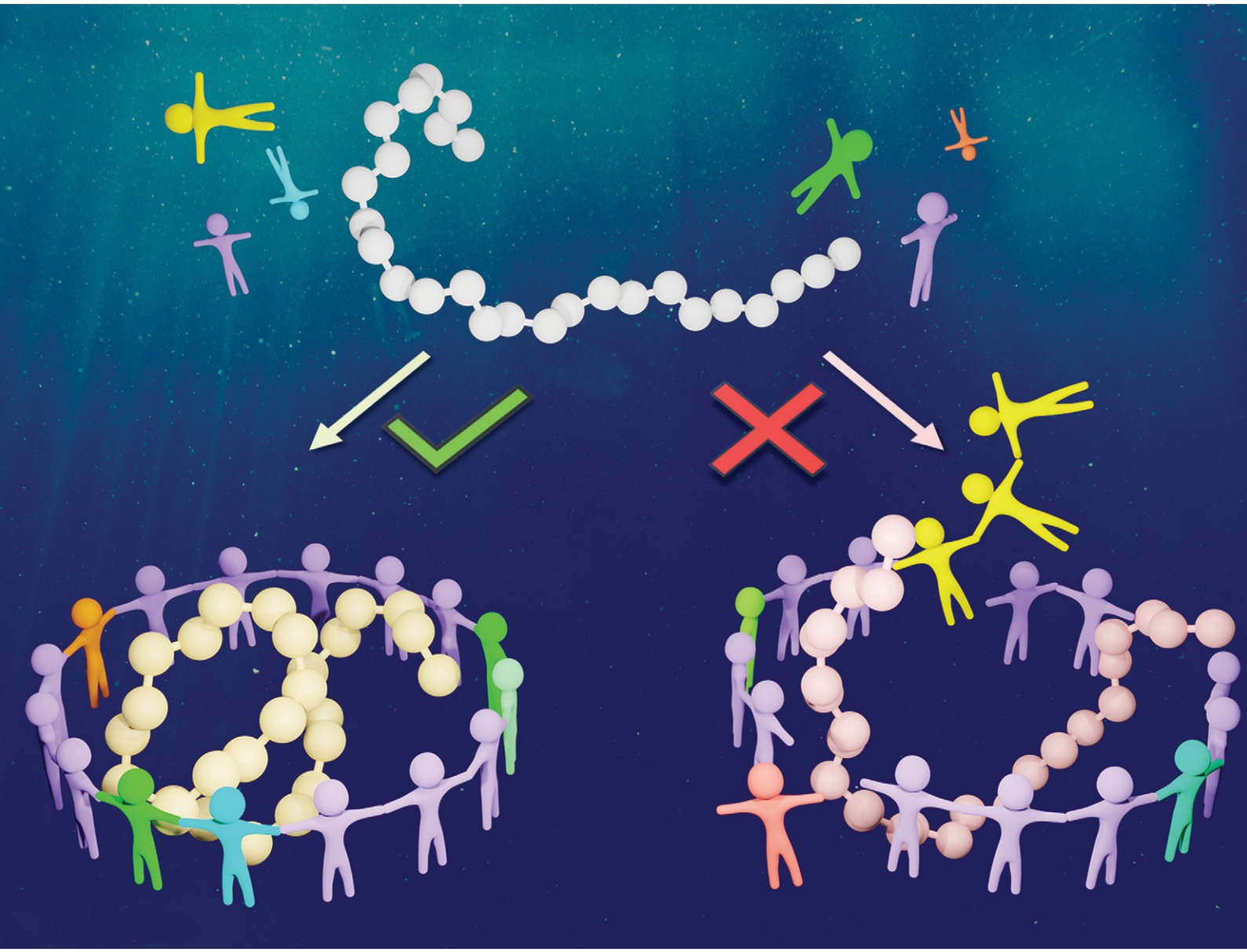

ISSN 2058-9689

ROYAL SOCIETY OF CHEMISTRY

PAPER

Sapna Sarupria *et al.*

Towards stable biologics: understanding co-excipient effects on hydrophobic interactions and solvent network integrity

IChemE ADVANCING CHEMICAL ENGINEERING WORLDWIDE

MSDE

PAPER

View Article Online
View Journal | View Issue

Cite this: *Mol. Syst. Des. Eng.*, 2025, 10, 432

Towards stable biologics: understanding co-excipient effects on hydrophobic interactions and solvent network integrity†

Jonathan W. P. Zajac, [ae] Praveen Muralikrishnan,[be] Caryn L. Heldt, [c] Sarah L. Perry [d] and Sapna Sarupria *[ae]

The formulation of biologics for increased shelf life stability is a complex task that depends on the chemical composition of both the active ingredient and any excipients in solution. A large number of unique excipients are typically required to stabilize biologics. However, it is not well-known how these excipient combinations influence biologics stability. To examine these formulations at the molecular level, we performed molecular dynamics simulations of arginine – a widely used excipient with unique properties – in solution both alone and with equimolar concentrations of lysine or glutamate. We studied the effects of these mixtures on a hydrophobic polymer model to isolate excipient mechanisms on hydrophobic interactions relevant in both protein folding and aggregation, crucial phenomena in biologics stability. We observed that arginine is the most effective single excipient in stabilizing hydrophobic polymer folding, and its effectiveness is augmented by lysine or glutamate addition. We decomposed the free energy of polymer folding/unfolding to identify that the key source of arginine–lysine and arginine–glutamate synergy is a reduction in destabilizing polymer–excipient interactions. We additionally applied principles from network theory to characterize the local solvent network embedding the hydrophobic polymer. Through this approach, we found arginine supports a more highly connected and stable local solvent network than in water, lysine, or glutamate solutions. These network properties are preserved when lysine or glutamate are added to arginine solutions. Taken together, our results highlight important molecular features in excipient solutions that establish the foundation for rational formulation design.

Received 20th December 2024,
Accepted 3rd March 2025

DOI: 10.1039/d4me00201f

rsc.li/molecular-engineering

Design, System, Application

Addition of excipient molecules to biological formulations is an effective strategy for improving the shelf life of biologics. Multiple unique excipients are typically required for a single formulation, however, the combinatorial effects of these excipients are rarely understood. In this work, we utilize molecular dynamics simulations of a hydrophobic polymer to resolve the effects of binary excipient formulations on a key aspect of biologics stability–hydrophobic interactions. A better understanding of co-excipient effects on this fundamental aspect of stability will lead to more efficient excipient selection during the formulation design process, saving both time and cost.

1 Introduction

Biologics are complex pharmaceutical products that often contain proteins.[1,2] The physicochemical stability of proteins—relevant in the shelf life of biologics—involves physical stability related to protein unfolding and aggregation, as well as chemical stability (*e.g.*, oxidation).[3–15] The most common strategy to increase stability involves lowering the storage temperature[16–20] and/or adding excipient molecules.[21–27]

Excipients are typically small molecules such as amino acids or sugars. Excipient selection in the development of biologics is a high-throughput and empirical process.[28–30] Excipients are deployed in combinations of four or more

[a] *Department of Chemistry, University of Minnesota, Minneapolis, MN 55455, USA. E-mail: sarupria@umn.edu*
[b] *Department of Chemical Engineering and Materials Science, University of Minnesota, Minneapolis, MN 55455, USA*
[c] *Department of Chemical Engineering, Michigan Technological University, Houghton, MI 49931, USA*
[d] *Department of Chemical Engineering, University of Massachusetts Amherst, MA 01003, USA*
[e] *Chemical Theory Center, University of Minnesota, Minneapolis, MN 55455, USA*

† Electronic supplementary information (ESI) available: Simulation details, error estimations, and additional analysis. See DOI: https://doi.org/10.1039/d4me00201f

unique molecules, on average.[27] This vast design space and a limited understanding of the combinatorial effects results in a time-consuming trial-and-error selection of compatible excipients, bottlenecking formulation development.[31] By some estimates, the development of novel excipients takes a long time frame of ~12 years, costing ~$35m in that span.[17,32,33] Understanding the molecular details of excipient mechanisms will aid in predicting optimal excipient selections for novel formulations, reducing both the time and cost associated with this stage of biologics production.

To gain molecular insights into excipient mechanisms, a reasonable strategy building toward predictive abilities would be to understand the effects of excipients on the key interactions (*e.g.*, hydrophobic, electrostatic, hydrogen bonding, *etc.*) that govern protein stability. Decoupling and studying the effects of excipients on specific interactions is non-trivial in wet-lab experiments. On the other hand, molecular dynamics (MD) simulations provide an excellent avenue to achieve this. We use a hydrophobic polymer that serves as a model for protein folding/unfolding[34–40] to probe the effect of excipients on hydrophobic interactions. Hydrophobic interactions are the driving and dominant interactions that govern protein folding and aggregation.[6,41–48] Thus, studies of hydrophobic interactions provide critical insight into the underlying mechanisms driving excipient behavior. For example, the denaturant urea weakens hydrophobic interactions,[35,38,49–54] while the stabilizing osmolyte trimethylamine *N*-oxide (TMAO) negligibly affects or strengthens these effects.[55–61]

As a starting point towards establishing excipient design rules, we turned our attention to a widely used excipient, arginine (Arg). Arg is a versatile excipient with a wide range of reported effects on protein stability. Arg is frequently used in protein and vaccine storage, purification techniques, and as an aggregation reducer.[22,62–66] However, in some contexts, Arg has been found to denature proteins,[67–69] accelerate aggregation,[70–72] and inactivate viruses.[40,73,74] In situations where Arg is denaturing, addition of charged co-excipients has been observed to reverse the denaturing properties of Arg.[68] In a separate context where Arg was found to be stabilizing, synergy was observed between Arg and glutamate (Glu) in the solubilization of model proteins.[75] Recently, we proposed that the multi-faceted effects of Arg arise from its positioning at the edge of a mechanistic flip between indirect- and direct-dominated mechanisms on hydrophobic interactions.[40] Due to its placement at this edge, we aimed to understand whether subtle changes in formulation composition alters the stabilizing properties of Arg. To this end, we investigated hydrophobic polymer folding in solutions of lysine (Lys), Glu, and Arg, as well as equimolar formulations of Arg/Lys, Arg/Glu, and Lys/Glu. We discovered that adding Lys or Glu to Arg/water solutions enhances hydrophobic polymer stability, underscoring the importance of co-excipient selection in protein folding and stability.

2 Methods

2.1 System setup and molecular dynamics simulations

To probe the effects of Arg, Lys, Glu, and binary excipient mixtures on hydrophobic interactions, we performed MD simulations of a hydrophobic polymer in excipient solutions at various concentrations. Replica exchange umbrella sampling (REUS)[76] simulations were utilized to calculate the potential of mean force (PMF) of hydrophobic polymer folding in different excipient solutions. The hydrophobic polymer was modeled as a linear coarse-grained chain with 26 monomers. Each monomer is represented as a bead with Lennard-Jones parameters σ = 0.373 nm and ε = 0.5856 kJ mol^{-1}.[55] The polymer–water ε parameter was modified to achieve an approximately even distribution of folded and unfolded polymer states in pure water.[40] Box dimensions were defined such that 1.5 nm of space separated the fully elongated polymer from the nearest box edge. All systems were solvated with roughly 10 000 TIP4P/2005 water molecules.[77] The salt forms of all excipients (Arg^+/Cl^-, Lys^+/Cl^-, Glu^-/Na^+) under study were added to the simulation box until the desired concentration was reached (Table S1†). The CHARMM22 force field was used to describe excipient molecules and ions.[78,79] With this protocol, we generated systems comprised of 0.25 M, 0.5 M, and 1.0 M Arg/water, Lys/water, Glu/water, Arg/Lys, Arg/Glu, and Lys/Glu. In binary excipient solutions, equimolar concentrations were used, with the total concentration kept constant.

All systems were energy minimized using the steepest descent algorithm. 1 ns NVT equilibration simulations were carried out at 300 K, followed by 1 ns NPT equilibration simulations at 300 K and 1 atm. During equilibration, temperature was controlled according to the *V*-rescale thermostat,[80] while pressure was controlled *via* the Berendsen barostat.[81] Following equilibration, NPT production runs were completed using the Nosé–Hoover thermostat (τ_T = 5 ps)[82] and Parrinello–Rahman barostat (τ_P = 25 ps).[83] Production runs were 20 ns long for excipient/water systems, and between 50–250 ns per window for excipient/polymer/water REUS simulations (Table S1†). Convergence was assessed by comparing PMFs as a function of simulation time and noting the point at which PMFs from three replicate simulations converged (Fig. S1†). The particle mesh Ewald (PME) algorithm was used for electrostatic interactions (cutoff = 1 nm). A reciprocal grid of 42 × 42 × 42 cells was used with 4th order B-spline interpolation. A single cutoff point of 1 nm was used for van der Waals interactions. The neighbor search was performed every 10 steps. Lorentz–Berthelot mixing rules[84,85] were used to calculate nonbonded interactions between different atom types. All simulations were run in GROMACS 2021.4.[86]

2.2 Replica exchange umbrella sampling (REUS)

REUS[76] simulations were performed to sample the hydrophobic polymer conformational landscape in excipient solutions. REUS simulations were done using GROMACS 2021.4 (ref. 86) with the PLUMED 2.8.0 (ref. 87 and 88) patch applied. The radius of

gyration (R_g) of the hydrophobic polymer was used as a reaction coordinate, placing 12 umbrella potential centers evenly between R_g = 0.3 nm and R_g = 0.9 nm. A force constant of K = 5000 kJ mol^{-1} nm^{-2} was used in all windows, with the exception of the window centered at R_g = 0.45 nm, which used K = 1000 kJ mol^{-1} nm^{-2}.[40]

The potential of mean force (PMF) of polymer folding/unfolding was calculated as $W(R_g) = -k_BT\ln(P(R_g))$. Biased probability distributions were reweighted according to the weighted histogram analysis method (WHAM).[89] The free energy of polymer unfolding (ΔG_u) was calculated according to:

$$\Delta G_u = -k_BT\ln\left(\frac{\int_{R_{g,cut}}^{R_{g,max}}\exp\left(\frac{-W(R_g)}{k_BT}\right)dR_g}{\int_{R_{g,min}}^{R_{g,cut}}\exp\left(\frac{-W(R_g)}{k_BT}\right)dR_g}\right) \quad (1)$$

where $R_{g,cut}$ was determined as the point between the folded and unfolded states where $\frac{\partial W(R_g)}{\partial R_g} = 0$. ΔG_u reflects the difference in free energy of the unfolded state relative to the folded state (*i.e.*, $\Delta G_u = G_{unfolded} - G_{folded}$).

We decomposed the PMF into individual components to further investigate the role of arginine in polymer folding. Following the methods outlined by several others,[40,90–93] the PMF was separated into intrapolymer degrees of freedom in vacuum, W_{vac}, and a solvent contribution, W_{solv} as:

$$W(R_g) = W_{vac}(R_g) + W_{solv}(R_g) \quad (2)$$

In accordance with perturbation theory approaches applied to solvation phenomena,[46,48,94–99] the solvent contribution can be described as involving two steps: (i) creating a polymer-sized cavity in solution ($W_{cav}(R_g)$), and (ii) turning on attractive polymer–solvent interactions ($E_{ps}(R_g)$). $W_{solv}(R_g)$, then, is computed as $[W(R_g) - W_{vac}(R_g)]$, resulting in:

$$W_{solv}(R_g) = W_{cav}(R_g) + E_{ps}(R_g) \quad (3)$$

where:

$$E_{ps}(R_g) = E_{pw}(R_g) + E_{pa}(R_g) + E_{pc}(R_g) \quad (4)$$

$E_{pw}(R_g)$, $E_{pa}(R_g)$, and $E_{pc}(R_g)$ are average polymer–water, polymer–amino acid, and polymer–counterion interaction energies, respectively, and correspond to the energy associated with a state change from folded to unfolded state. From eqn (2) and (3), $W_{cav}(R_g) = W(R_g) - W_{vac}(R_g) - E_{ps}(R_g)$. $W_{vac}(R_g)$ is obtained from independent REUS simulations of the polymer in vacuum. All interaction energies were computed using the *gmx rerun* feature of GROMACS, defining separate energy groups for polymer, amino acid, counterion, and water.

2.3 Preferential interaction coefficients

Distribution of water and excipient molecules with respect to any solute can be quantified *via* the preferential interaction coefficient, Γ_{PA}.[100–102] This parameter is calculated in simulations using the two-domain formula:[103–105]

$$\Gamma_{PA} = \left\langle N_A^{local} - \left(\frac{N_A^{bulk}}{N_W^{bulk}}\right)N_W^{local}\right\rangle \quad (5)$$

where P denotes the polymer, A represents an additive species (Arg, Lys, Glu, Na^+, or Cl^-), and W denotes water. N represents the number of molecules of a given species, while angular brackets denote an ensemble average. The local and bulk domain was separated by a cutoff distance R_{cut} from the polymer. Γ_{PA} gives a measure of the relative accumulation or depletion of an additive in the local domain of the hydrophobic polymer; $\Gamma_{PA} > 0$ indicates relative accumulation (preferential interaction) and $\Gamma_{PA} < 0$ indicates relative depletion (preferential exclusion).

Wyman–Tanford theory relates any equilibrium process and preferential interaction as:[106–108]

$$-\left(\frac{\partial\Delta G_u}{\partial\mu_A}\right) = \Gamma_{PA}^u - \Gamma_{PA}^f \quad (6)$$

Consistent with this relationship, denaturants have shown to have a greater preferential interaction coefficient in the unfolded ensemble and stabilizing molecules have a greater preferential interaction coefficient in the folded ensemble.[37,109–111] Here, we use this framework to connect preferential interactions in the unfolded (Γ_{PA}^u) and folded (Γ_{PA}^f) ensembles to the observed excipient stabilizing effects.

2.4 Arginine clustering

Several studies have identified the importance of Arg clustering in the multi-faceted effects of the excipient.[74,112–118] As a free molecule, Arg forms self-associated clusters *via* three primary interactions: (i) backbone–backbone (COO^-–NH_3^+), (ii) backbone–sidechain (Gdm^+–COO^-), and (iii) sidechain–sidechain (Gdm^+–Gdm^+). To quantify the extent of Arg cluster formation, we applied the following geometric criteria for the interactions defined above between pairs of molecules i and j, where $i \neq j$: (i) at least one COO^- oxygen from i within 2.0 Å of an NH_3^+ hydrogen from j, (ii) at least one COO^- oxygen from i within 2.0 Å of a Gdm^+ hydrogen from j, and (iii) at least one Gdm^+ carbon from i within 4.0 Å of a Gdm^+ carbon from j.

For binary excipient solutions, criteria (i) and (ii) may be met *via* the sidechains of Glu and Lys, which introduce additional COO^- and NH_3^+ groups into the system, respectively. Criterion (iii) may only be achieved *via* two interacting Arg molecules. For every excipient molecule i in solution, we iteratively searched over every other excipient molecule j. Molecules found to match the criteria outlined above were used to construct individual graphs, g_i, with a central node positioned on molecule i and edges connecting i to all interacting residues j. NetworkX[119] was used to merge any individual graphs with shared edges into clusters. The largest cluster size is reported as the maximum value of elements within any of the c_i constructed clusters.

To characterize excipient clusters according to interaction types, we computed an interaction efficiency metric, η, according to:

$$\eta = (n_k/N_k) \times 100 \tag{7}$$

where n_k is the number of contacts observed that match criteria k, and N_k is the total number of all excipient molecules that can participate in criteria k. For criteria (i) and (ii), N_k denotes the total number of excipient molecules in solution, while for (iii), N_k denotes the total number of Arg molecules, as only Arg molecules can satisfy this criterion.

2.5 Network analysis

Several techniques from network theory were applied to quantify the solvent structure of the local polymer domain. Graphs, $G(t)$, were constructed for a configuration at time t using NetworkX.[119] Nodes were defined as any solvent molecule (which includes either water or excipient) center-of-mass within 0.7 nm of the hydrophobic polymer. An edge was constructed between nodes if a pair of heavy atoms i and j, belonging to solvent molecules I and J, were within 0.35 nm of each other. Network analysis was performed on configurations taken every 100 ps from the REUS trajectories.

We used the Wasserman and Faust improved formula to calculate closeness centrality for all nodes in the graph:[120,121]

$$C_c(u) = \frac{n-1}{N-1}\left(\frac{n-1}{\sum_{v=1}^{n-1} d(u,v)}\right) \tag{8}$$

where n is the number of reachable nodes from node u, and N is the total number of nodes in the graph, $G(t)$. $d(u, v)$ is the shortest distance between node u and reachable node v. A reachable node refers to any node that is accessible to node u through a continuous sequence of connected nodes. Betweenness centrality was measured as:[121–123]

$$C_b(u) = \sum_{s,t} \frac{n_p(s, t|u)}{n_p(s, t)} \tag{9}$$

where $n_p(s, t)$ is the number of shortest paths between nodes s and t through the connected network, and $n_p(s, t|u)$ is the number of such paths that pass through node u. Further, by assigning nodes as either belonging to excipient molecules or water molecules, we decomposed these quantities into water centrality (C^{wat}) and excipient centrality (C^{exc}) measurements.

We measured graph stability by computing a fragmentation threshold, f. In this approach, we began with all complete graphs $G(t)$ for which the number of independent graphs was equal to 1. Iteratively, we randomly removed individual nodes and any associated edges from the graph. At each step, the number of disconnected graphs was computed, and the point at which this value changed from 1 to 2 was recorded as the fragmentation threshold. This point is equivalent to the critical point at which a lattice reaches catastrophic failure, resulting in its collapse.[124] In practice, we report this value as the fraction of nodes removed, $f = u/U$, where u is the number removed and U is the total number of nodes in the graph. Because the fragmentation threshold will be sensitive to the sequence through which nodes are removed, we performed 100 iterations of our random node removal algorithm per configuration, and report the average value of f.

In addition to the stochastic node removal algorithm described above, we explored the effect of removing only nodes that are continuously connected to one another. For example, following removal of node s, the options for sequential node removal are only neighboring nodes $t(s)$. We refer to this approach as continuously connected node removal, which can be thought of as identifying more optimal pathways for solvent network fragmentation.

2.6 Hydration shell dynamics

The rotational dynamics of water was measured by computing the characteristic reorientation time of the water dipole vector, μ.[118,125,126] This dipole was taken as the vector connecting the oxygen atom and the center of the two hydrogen atoms of a water molecule. The time evolution of this vector was monitored by computing the time correlation function:

$$C_\mu(t) = \frac{\langle \mu_i(0)\cdot\mu_i(t)\rangle}{\langle \mu_i(0)\cdot\mu_i(0)\rangle} \tag{10}$$

where $\mu_i(t)$ is the dipole vector of the ith water molecule at time t. Water molecules were considered for analysis according to the following protocol (Scheme S1†): (i) the Cartesian coordinates of the water oxygen is within r to $r + dr$ at $t = 0$, (ii) if a water molecule moves into a buffer region, spanning $r + dr$ to $r + dr + b$, its position is flagged and tracked over time, and (iii) a water molecule is removed from consideration if the tracked molecule exits the buffer region without re-entry into the r to $r + dr$ shell, or persists within the buffer region for at least 2 ps. In the above criteria, r denotes the minimum distance from the center of the nearest hydrophobic polymer bead, dr is the width of the hydration layer under consideration, and b is the width of the buffer region.

Unbiased MD simulations were performed for water dynamics analyses. Configurations from the folded and unfolded ensemble obtained from the REUS simulations were clustered using HDBSCAN[127] (Fig. S2 and S3†). Representative configurations corresponding to the highest cluster membership probability were then used to start the unbiased simulations. The unbiased simulations were performed for 300 ps in the NPT ensemble and configurations were stored every 0.1 ps.

3 Results and discussion

The goal of this study is to elucidate the mechanisms underpinning the stabilization of biological formulations by amino acids. To this end, we examined the effects of single

excipient solutions of the amino acids Arg, Lys, Glu, and their binary mixtures on the stability of a model hydrophobic polymer.

3.1 High concentrations of excipients favor folding of a hydrophobic polymer

The free energy of hydrophobic polymer unfolding in excipient solutions is reported in Fig. 1. At 0.25 M concentration, hydrophobic polymer folding is favored in Arg/water solutions ($\Delta G_u > 0$), while unfolding is favored in Lys/water and Glu/water solutions ($\Delta G_u < 0$). At 0.5 M and 1.0 M concentrations, Arg/water, Lys/water, and Glu/water solutions favor hydrophobic polymer folding. At all concentrations, Arg is the most effective single excipient in stabilizing the folded hydrophobic polymer state. Lys is the next most effective excipient, while Glu is the least effective.

Among binary excipient mixtures, both Arg/Glu and Arg/Lys stabilized the folded polymer state, with stability increasing with concentration (Fig. 1). Our results indicate that 1.0 M Arg/Lys and Arg/Glu mixtures are synergistic relative to their single excipient solutions, as the free energy of polymer unfolding in these solutions is less favorable than in any single excipient solution. In Lys/Glu mixtures, hydrophobic polymer folding is favored at 0.25 M, whereas the unfolded polymer is favored in Lys/water and Glu/water solutions at this concentration. Hence, we identify Lys/Glu mixtures to be synergistic at 0.25 M, although at higher concentrations this synergy is not observed.

3.2 Thermodynamic components of hydrophobic polymer folding in excipient solutions

To explore the thermodynamic origins of the excipient effects on hydrophobic polymer folding, we decomposed the PMF into components as discussed in eqn (4). Fig. 2 shows the change in each component upon unfolding in an excipient solution relative to that observed in water. The first Δ arises from the difference between folded and unfolded states (*e.g.*, $\Delta E = \langle E_u \rangle - \langle E_f \rangle$), and the second Δ arises from the difference between the excipient solution (ΔE_{exc}) and water (ΔE_{wat}) (*e.g.*, $\Delta\Delta E = \Delta E_{exc} - \Delta E_{wat}$). In all cases, we found $\Delta\Delta G_{vac} \approx 0$, as W_{vac} does not depend on the solvent. Additionally, the change in polymer–counterion interaction energy, $\Delta\Delta E_c$, was observed to be near 0 in all cases. Hence, these terms were omitted from Fig. 2 for clarity.

In Arg/water solutions and at low concentrations, direct polymer–Arg interactions favor folding, while at high concentrations, the cavity component and polymer–water interactions drive folded state stability.[40] For Glu/water (Fig. 2b) and Lys/water (Fig. 2c) solutions, polymer folding is favored with increasing concentration. This is driven primarily by a favorable cavity component, while polymer–Glu and polymer–Lys interactions oppose folding. The polymer–water component is negligible in Lys/water and Glu/water solutions.

For binary mixtures, Arg/Glu (Fig. 2d) and Arg/Lys (Fig. 2e), direct polymer–amino acid interactions favor polymer folding at 0.25 M and 0.5 M, while at 1.0 M, this contribution is negligible. In contrast, the cavity component and polymer–water interactions favor polymer unfolding at 0.25 M and 0.5 M, while these components favor polymer folding at 1.0 M. In the case of Lys/Glu (Fig. 2f) solutions, stabilization of the folded polymer is almost fully determined by the cavity component. A monotonic increase in this component is observed with increasing Lys/Glu concentration, while polymer–water and polymer–amino acid interactions are negligible.

3.3 Excipient synergy is driven by changes in direct interactions

To quantify the extent of synergy (and non-ideality) in binary excipient mixtures, we computed the excess unfolding free energy (ΔG_u^{excess}) as:

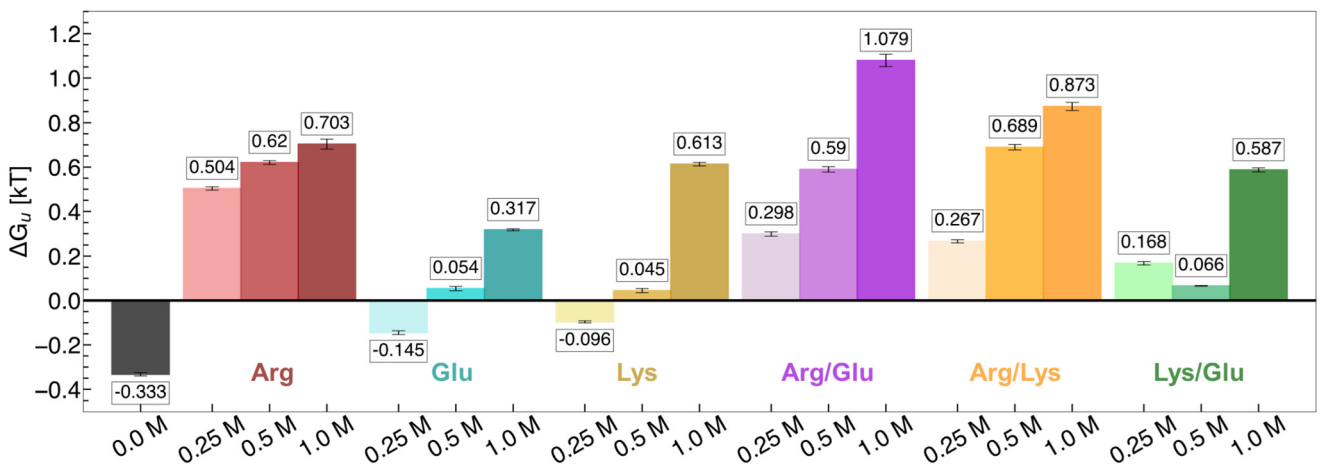

Fig. 1 Free energy of hydrophobic polymer unfolding in Arg, Glu, Lys, Arg/Glu, Arg/Lys, and Lys/Glu solutions. Increasing excipient concentration is denoted by increased shading (light to dark; left to right). Mean values are reported from three replicate REUS simulations. Error bars were estimated *via* error propagation (see ESI† for details).

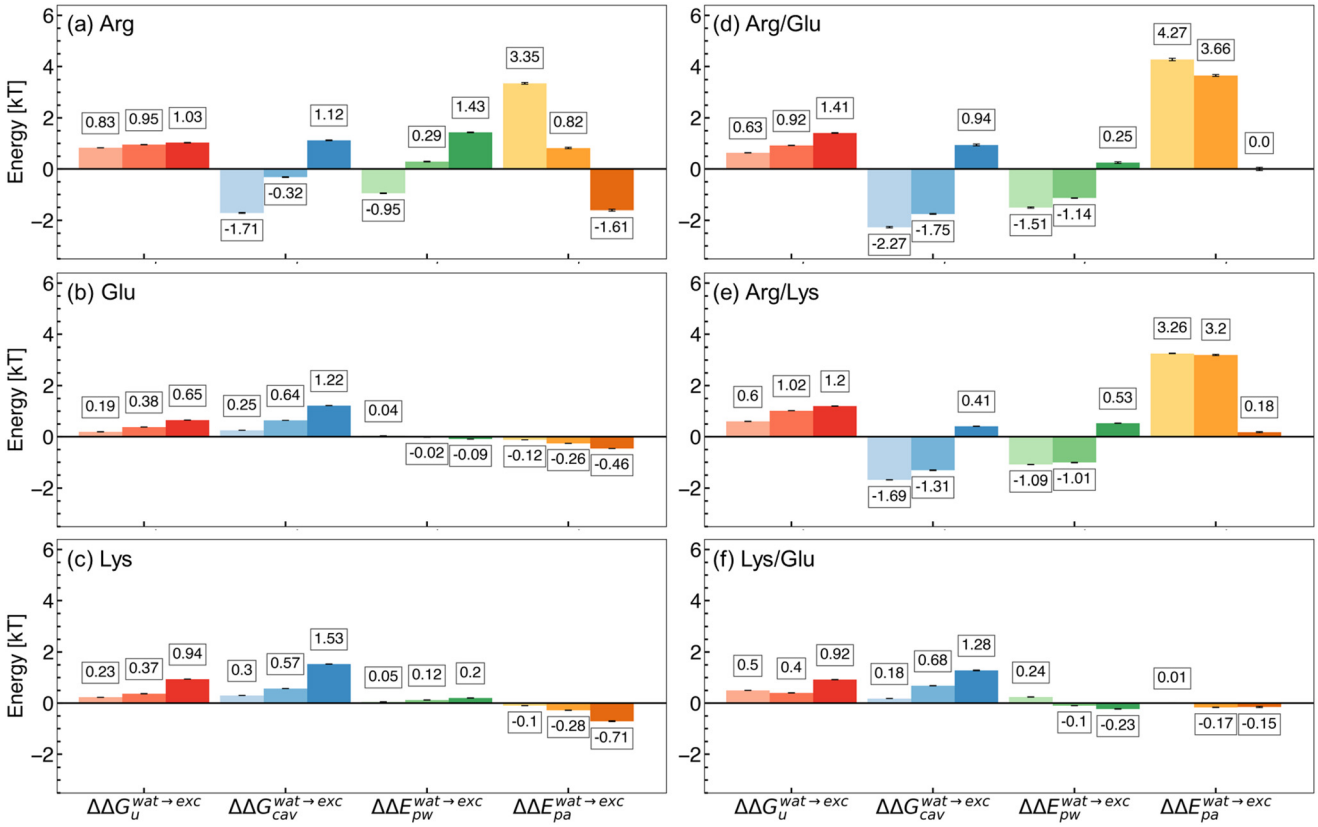

Fig. 2 Contributions to the free energy of hydrophobic polymer unfolding in excipient solutions relative to water. (a) Arg/water, (b) Glu/water, (c) Lys/water, (d) Arg/Glu, (e) Arg/Lys, and (f) Lys/Glu solutions. Changes in free energy of unfolding ($\Delta\Delta G_u$), cavitation contribution ($\Delta\Delta G_{cav}$), polymer–water interactions ($\Delta\Delta E_{pw}$), and polymer–amino acid interactions ($\Delta\Delta E_{pa}$) are shown. Increasing additive concentration is denoted by increased shading (light to dark; left to right). Mean values are reported from three replicate REUS simulations. Error bars were estimated *via* error propagation (see ESI† for details).

$$\Delta G_u^{excess} = \Delta G_u^{mix} - \Delta G_u^{ideal} \quad (11)$$

where $\Delta G_u^{ideal} = x_a \Delta G_u^a + x_b \Delta G_u^b$ for excipients a and b in mole fractions x_a and x_b respectively. ΔG_u^a and ΔG_u^b represent the unfolding free energy in solutions of single excipients a or b, respectively. ΔG_u^{mix} represents the free energy of unfolding of binary excipient solution a and b at the same total concentration. In cases where $\Delta G_u^{excess} > 0$, the binary excipient mixtures have a more favorable effect on hydrophobic polymer folding than the ideal reference mixture. To probe the mechanistic underpinnings of this synergy, we investigate both direct interactions (polymer–amino acid and polymer–counterion; ΔG_{dir}^{excess}) and indirect effects (cavitation and polymer–water; ΔG_{ind}^{excess}) associated with each solution (Fig. 3).

In all binary excipient solutions, we observe favorable changes ($\Delta G_u^{excess} > 0$) in the free energy of polymer unfolding, relative to single excipient solutions. In Arg/Glu (Fig. 3a) and Arg/Lys (Fig. 3b) solutions, this increased folding state favorability is associated with a favorable change in direct polymer–amino acid interactions. At the same time, folded state stability is opposed by unfavorable indirect components, relative to in single excipient solutions. The same observations are made for Lys/Glu (Fig. 3c), albeit to a lesser extent. Interestingly, a different optimal concentration (with maximal ΔG_u^{excess}) is observed for each pair of excipients – 1.0 M for Arg/Glu, 0.5 M for Arg/Lys, and 0.25 M for Lys/Glu.

The manifestation of the observed synergy describes a mechanism for improving the effectiveness of Arg-containing solutions. We observe that, while Arg is effective in stabilizing hydrophobic polymer folding, attractive polymer–Arg interactions drive unfolding at 1.0 M concentration. In the presence of Lys or Glu, this opposition to folding is eliminated. Hence, co-excipient addition is a suitable strategy to alter excipient effects on hydrophobic polymer folding.

Co-excipient synergy results from a re-balancing of polymer–water–excipient interactions. This balance is captured by the preferential interaction coefficient, Γ_{PA}. $\Gamma_{PA} > 0$ indicates relative accumulation of an excipient (and a corresponding depletion of water) in the local polymer domain, while $\Gamma_{PA} < 0$ indicates relative depletion (and corresponding preferential hydration). In Fig. 4, we report Γ_{PA} for the excipient solutions in this study. We find Arg preferentially interacts with the hydrophobic polymer (Fig. 4a), while Glu (Fig. 4b) and Lys (Fig. 4c) are preferentially excluded. These trends increase with concentration.

We explored the change in excipient distribution by considering Γ_{PA} of an excipient when in a single excipient *versus* binary excipient solution. In Fig. 4d–f, we show

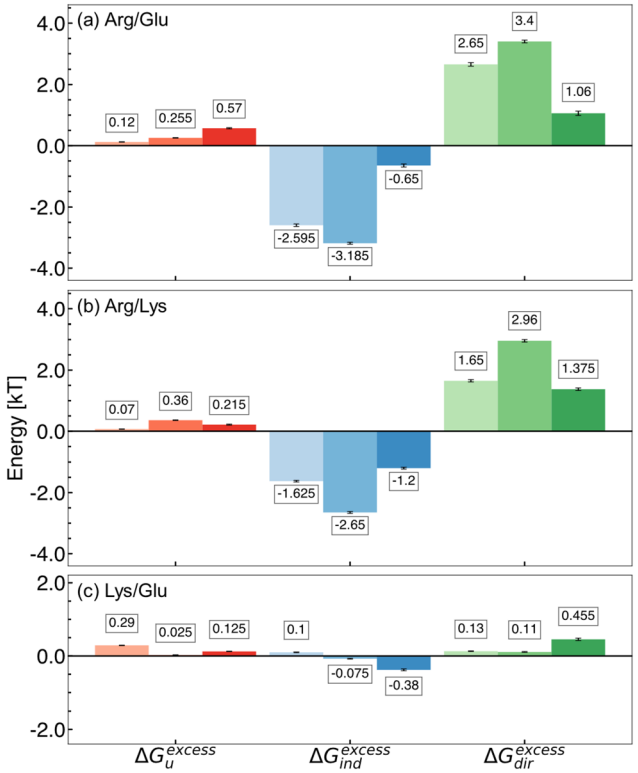

Fig. 3 Excipient synergy observed in 0.25 M, 0.50 M, and 1.0 M (a) Arg/Glu, (b) Arg/Lys, and (c) Lys/Glu solutions. Changes in overall free energy of unfolding (ΔG_u^{excess}), direct interactions (ΔG_{dir}^{excess}), and indirect interactions (ΔG_{ind}^{excess}) and polymer are shown. Increasing additive concentration is denoted by increased shading (light to dark; left to right). Mean values are reported from three replicate REUS simulations. Error bars were estimated *via* error propagation (see ESI† for details).

ensemble averaged Γ_{PA} values using an R_{cut} value of 0.7 nm. This value is selected as a cutoff distance because, beyond this distance, no significant changes in Γ_{PA} are observed for the excipients (Fig. S5†). From this perspective, the preferential accumulation of Arg near the polymer is reduced in Arg/Lys or Arg/Glu solutions, relative to in Arg/water solutions (Fig. 4d). We have previously highlighted that, at 1.0 M Arg concentration, direct polymer–Arg interactions drive unfolding.[40] Hence, we hypothesize that a reduction in polymer–Arg interactions upon Lys or Glu incorporation in the solution results in net stabilization of the folded hydrophobic polymer.

Alongside the changes in Arg distribution, the relative accumulation of Lys or Glu is increased in Arg/Lys and Arg/Glu solutions, relative to in single excipient solutions (Fig. 4e and f). Overall, these findings imply a mutual recruitment of excipient A into the preferred domain of excipient B in binary excipient solutions.

The change in Γ_{PA} observed in binary excipient solutions describes, in part, the effects observed in Fig. 3. In Arg/Glu and Arg/Lys solutions, there is a depletion in Γ_{PA}^{Arg} relative to in Arg/water, resulting in a net reduction of polymer–amino acid interactions. Correspondingly, a favorable change in the direct component, ΔG_u^{excess}, arises in Arg/Glu and Arg/Lys solutions, conferring increased stabilization of hydrophobic polymer folding.

3.4 Stabilizing co-excipients preserve the network effects of Arg

Networks of excipient–water interactions embedding the hydrophobic polymer were analyzed using principles of network theory. In this approach, we treat the center-of-mass of all excipient and water molecules within 0.7 nm of any polymer bead as nodes. A 0.7 nm cutoff was selected because, beyond this distance, the ratio of excipient to water molecules remained approximately constant. Edges are constructed between nodes

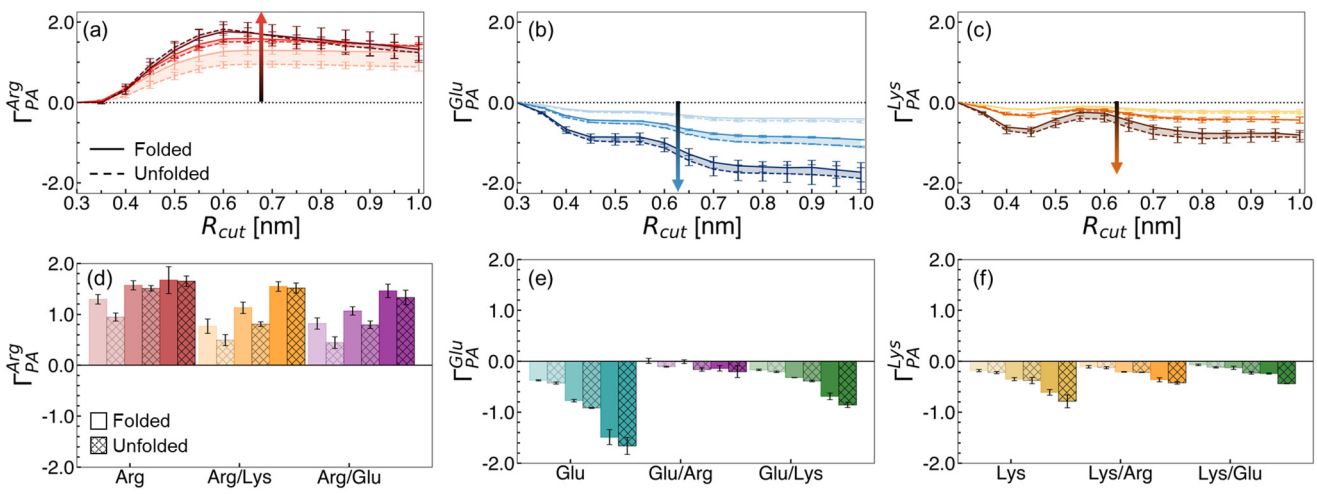

Fig. 4 Preferential interaction coefficient values as a function of the cutoff distance for the local domain of the hydrophobic polymer for (a) Arg, (b) Glu, and (c) Lys. Changes in Γ_{PA} at R_{cut} = 0.7 nm are shown for (d) Arg mixtures, (e) Glu mixtures, and (f) Lys mixtures. Solid lines indicate values for the folded state, while dashed lines in (a–c) and hatches in (d–f) denote values obtained from unfolded configurations. Increasing concentration is denoted by increased shading (light to dark). Arrows denote the trend with increasing concentration in (a–c). Mean values and errors were estimated from three replicate simulations. Errors are reported as standard deviations from mean values.

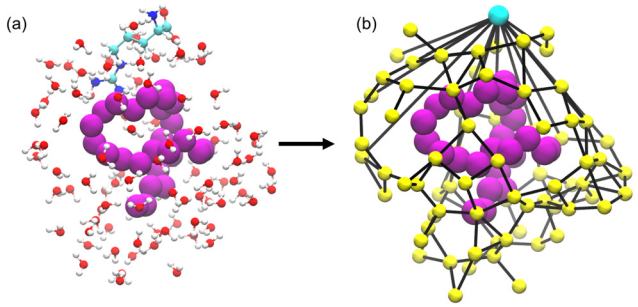

Fig. 5 Graph/network representation of the hydrophobic polymer local environment. (a) Representative snapshot taken from a REUS trajectory. (b) Graph representation of the snapshot in (a). The hydrophobic polymer, which is not included in the graph but is added here for illustration, is represented by purple spheres. Water nodes in the local polymer domain are colored yellow, while an excipient node is colored in cyan. Edges between connecting nodes are drawn as black lines.

where any pair of heavy atoms are located within 0.4 nm of one another (Fig. 5). To quantify the flow of molecular interactions within the solvent network, we measured closeness centrality,[120,121] C_c, and betweenness centrality,[121–123] C_b. Closeness centrality can be regarded as a measure of how long it takes to spread information from node u to all other nodes sequentially. Correspondingly, this quantity is a measure of how close a node is to the center of the network. Betweenness centrality quantifies the number of times a node acts as a bridge along the shortest path between two other nodes. In other words, this quantity measures the propensity for a node to act as a "hub" of information propagation. For both measurements, we resolve centrality from all water or excipient nodes.

Distributions of centrality measurements obtained from folded state configurations are shown in Fig. 6. Distributions from unfolded configurations result in qualitatively similar trends to folded configurations (Fig. S5 and S6†), and hence were omitted from Fig. 6, for clarity. In Arg/water solutions, we observe an increase in water closeness centrality (C_c^{Wat}) (Fig. 6a) and a decrease in water betweenness centrality (C_b^{Wat}) (Fig. 6b). The increase in C_c^{Wat} indicates shorter distances from water nodes to all other nodes – in other words, in Arg/water solutions, connectivity is increased among water molecules. This observation supports previous attempts to describe excipient effects *via* a network-based approach, which found that proteins in solution with stabilizing excipients have more compact interaction networks relative to those in the presence of denaturants.[128]

The decrease in C_b^{Wat} suggests water molecules do not act as key transmitters within the local solvent network. Correspondingly, relatively high excipient betweenness (C_b^{Exc}) distributions are observed for Arg/water solutions (Fig. 6d). This conveys that Arg molecules integrate well into the local polymer environment, acting as central hubs for information transfer in the local solvent structure. Elsewhere, it has been reported that stabilizing osmolytes have similarly high betweenness centrality values.[129] Taken together, this indicates that having a well-connected local solvent environment promotes excipient-driven stability of biologics.

Network analysis reveals several key differences between Lys/water and Glu/water solutions relative to Arg/water solutions. In Lys/water and Glu/water, both C_c^{Wat} and C_b^{Wat} are found to

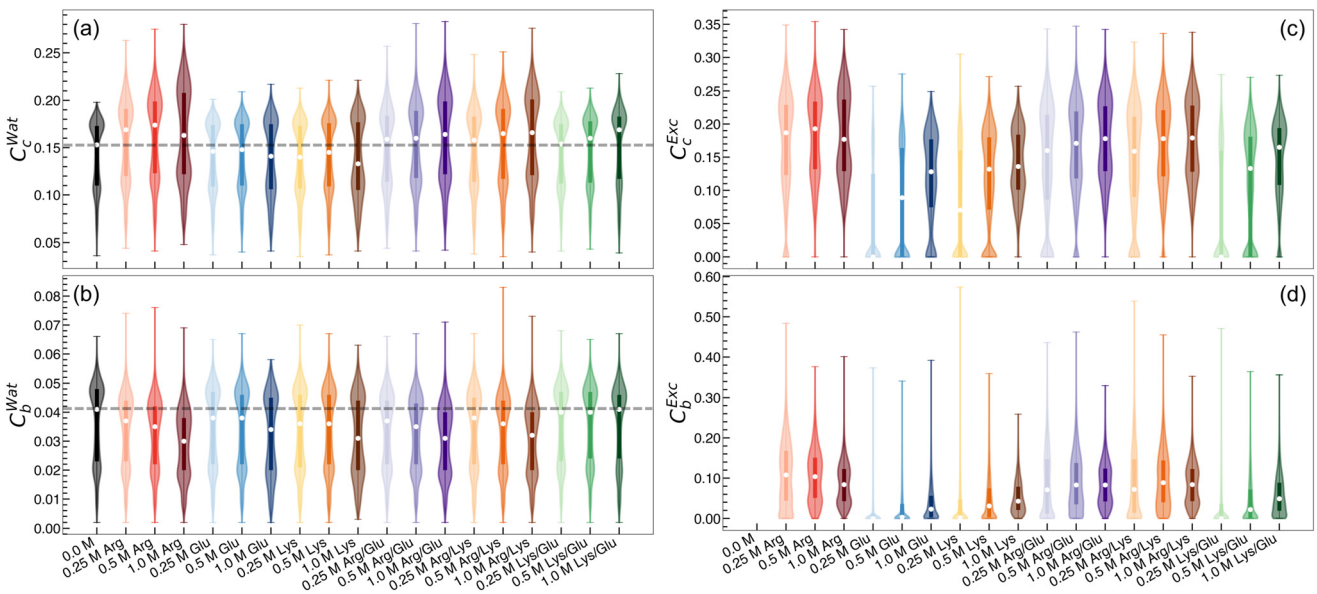

Fig. 6 Violin plots of centrality measurements for the network representing the local polymer environment for folded configurations. (a) Closeness centrality among water nodes. (b) Betweenness centrality among water nodes. (c) Closeness centrality among excipient nodes. (d) Betweenness centrality among excipient nodes. Mean values are denoted by white dots. In (a) and (b), the horizontal dashed line marks the mean centrality values for polymer + water solution.

decrease, or at least result in negligible changes relative to polymer–water systems. This suggests that water molecules become less connected within the local solvent environment network (Fig. 6a), while also becoming less essential hubs for information propagation (Fig. 6b). In contrast to Arg/water solutions, C_c^{Exc} and C_b^{Exc} are both relatively low, implying that Lys and Glu do not integrate into the local solvent environment as well as Arg (Fig. 6c and d). These results are consistent with our preferential interaction coefficient analysis, with the additional takeaway that connectivity among water molecules is reduced in Lys/water and Glu/water solutions.

Overall, we observe strongly connected networks in Arg/water solutions, and networks with poor connectivity in Lys/water and Glu/water solutions, relative to Arg solutions. In binary excipient solutions containing Arg (Arg/Lys and Arg/Glu), we observe an overall preservation of the strong connectivity identified in Arg solutions alone. Specifically, C_c^{Wat} is found to increase in Arg/Lys and Arg/Glu solutions relative to polymer/water systems, reflecting increased connectivity among water molecules (Fig. 6a). Similar to Arg/water solutions, C_b^{Wat} is observed to decrease with a concomitant increase in C_b^{Exc}, reflecting favorable integration of excipient molecules into the local polymer environment in Arg/Lys and Arg/Glu solutions (Fig. 6b and d). Finally, C_c^{Exc} is consistently higher in Arg/Lys and Arg/Glu solutions relative to Lys/water and Glu/water, marking an increase in local excipient connectivity in these binary excipient solutions (Fig. 6c). In general, the Lys/Glu binary excipient solution reflects network properties similar to Lys/water or Glu/water solutions.

We hypothesize that solutions with stronger connectivity in the solvent environment local to the hydrophobic polymer may confer greater stability to the network itself. To assess this, we compute a fragmentation metric, f, which measures the average number of nodes that must be removed from a fully-connected graph of the local solvent environment to form disconnected graphs. This metric corresponds to the point where it becomes impossible to transfer information throughout the entire local solvent environment. Our approach is inspired by percolation theory, and has been used elsewhere to measure the stability of large biomolecular assemblies, including viral capsids.[130,131] To our knowledge, this is the first time such an approach has been used to measure the network stability of a local solvent environment.

To better quantify differences in fragmentation distributions, we computed the Earth mover's distance (EMD)[132] as a measure of distribution dissimilarity, where higher EMD values indicate less overlap between two distributions. On average, local polymer environments are more resistant to fragmentation in Arg/water, Arg/Lys, and Arg/Glu solutions (Fig. 7a and S8a†), as indicated by increasing f distributions and relatively large EMD values. For all solutions, f values are higher in the local environments of folded polymer states, relative to unfolded polymer states (Fig. S8b†). However, this appears to be a general trend, as the differences between folded state and unfolded state graph stability do not depend on solution identity (Fig. 7b). We also observed qualitatively similar trends between

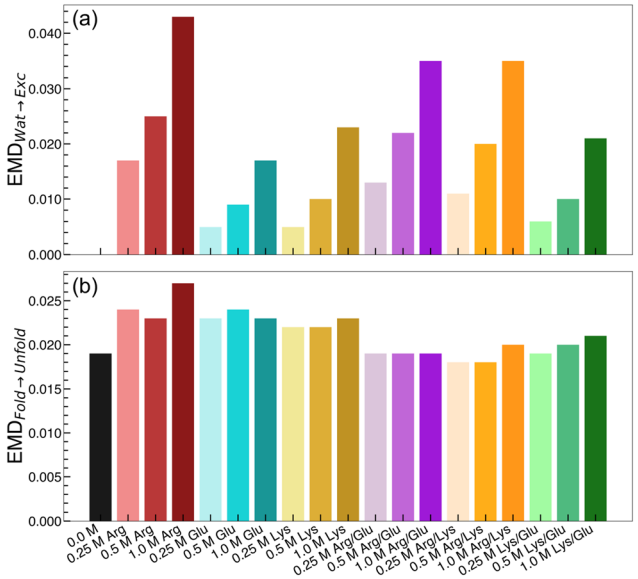

Fig. 7 Graph fragmentation analysis of the local hydrophobic polymer environment. (a) Earth mover's distance (EMD) between the 0.0 M fragmentation threshold distribution and a given excipient distribution, for folded polymer configurations. (b) EMD between folded and unfolded state fragmentation threshold distributions for all solutions.

stochastic node removal and continuously connected node removal (Fig. S8c†). Intuitively, we could consider the pathways that lead to fragmentation with the least number of nodes removed as the optimal pathways for local solvent network fragmentation. All f distributions are observed to decrease following continuously connected node removal, which indicates that continuous fragmentation results in faster disruption of the solvent network. We also noticed that the difference between folded and unfolded state f values ($\Delta f = f^{fold} - f^{unfold}$) decreased when changing from stochastic to continuously connected node removal ($\Delta\Delta f = f^{continuous} - f^{stochastic}$) (Fig. S8d†). For Glu, Lys, Arg/Glu, Arg/Lys, and Lys/Glu, this $\Delta\Delta f$ value increases with concentration, which we interpret as an indication that random node removal results in a fragmentation pathway further from the optimum in a given excipient solution. For these solutions, this deviation from optimal fragmentation increases with concentration. The inverse appears to be true for Arg—as more Arg is added, the difference between a randomly generated fragmentation pathway and the optimal fragmentation pathway becomes smaller. We may interpret this as Arg naturally forming more fragmentation–prone pathways within the local solvent network. Addition of Lys or Glu to Arg solutions, then, appears to reduce the probability of observing these fragmentation–prone configurations.

3.5 Explaining co-excipient synergy

Overall, we have uncovered that Arg/water solutions stabilize hydrophobic polymer folding to a greater extent than Lys/water, Glu/water, or Lys/Glu solutions. Addition of Lys or Glu to Arg/

water solutions gives rise to synergistic effects, as the resulting Arg/Lys and Arg/Glu solutions are the most effective stabilizing solutions in this study. These synergies are associated with stabilizing indirect effects at high concentrations and a dramatic reduction in destabilizing direct interactions. Correspondingly, the solvent distribution, as characterized by preferential interaction coefficient analysis, reflects a reduction in Arg accumulation in the local hydrophobic polymer domain with addition of Lys or Glu.

Network analysis implies that Arg integrates well into the local polymer environment, increases connectivity among water molecules, and increases the stability of the solvent network embedding the hydrophobic polymer. Importantly, these key network properties persist for Arg/water solutions to a greater extent than in Lys/water and Glu/water solutions. Moreover, the addition of Lys or Glu to Arg/water solution preserves the network properties of Arg/water alone, which may be a key aspect giving rise to the observed synergy among these excipients.

Based on these observations, we hypothesize that the addition of Lys or Glu to Arg/water solutions results in the formation of the same stable, highly connected local polymer environment as in solutions containing only Arg, while simultaneously reducing the penalty associated with direct polymer–Arg interactions. To better understand the unique roles played by Lys or Glu in this observed synergy, additional analyses were carried out.

3.5.1 Explaining Arg/Lys synergy: the sticky guanidinium hypothesis. Given the importance of excipient–excipient interactions in dictating solution structure, we aimed to explore these molecular interactions further. In particular, Arg–Arg clustering has been implicated as a key feature associated with the multi-faceted effects of Arg as an excipient.[74,112–118] Amino acid excipients in this study can interact in solution *via* three primary modes: (i) backbone–backbone (COO^-–NH_3^+), (ii) backbone–sidechain (Gdm^+–COO^-), and (iii) sidechain–sidechain (Gdm^+–Gdm^+). Using the geometric criteria for identifying these specific interactions, we analyzed excipient cluster formation in different excipient solutions.

Overall, the extent of cluster formation, as measured by the average largest cluster size, is greater in Arg/water and Arg/Glu solutions than in Arg/Lys (Fig. 8a). We attribute this finding to favorable electrostatic interactions between Arg and Glu, as well as the unique properties of the Gdm^+ sidechain of Arg that enable favorable like-charge interactions.[114,133–136] The presence of cluster formation in all Arg-containing solutions is primarily driven by Gdm^+–COO^- interactions (Fig. 8b and c), a finding consistent with previous work detailing the importance of Arg "head-to-tail" stacking.[114] Interestingly, while excipient clustering is reduced overall in Arg/Lys solutions relative to Arg/water, the extent of Gdm^+–Gdm^+ pairing among Arg molecules is increased.

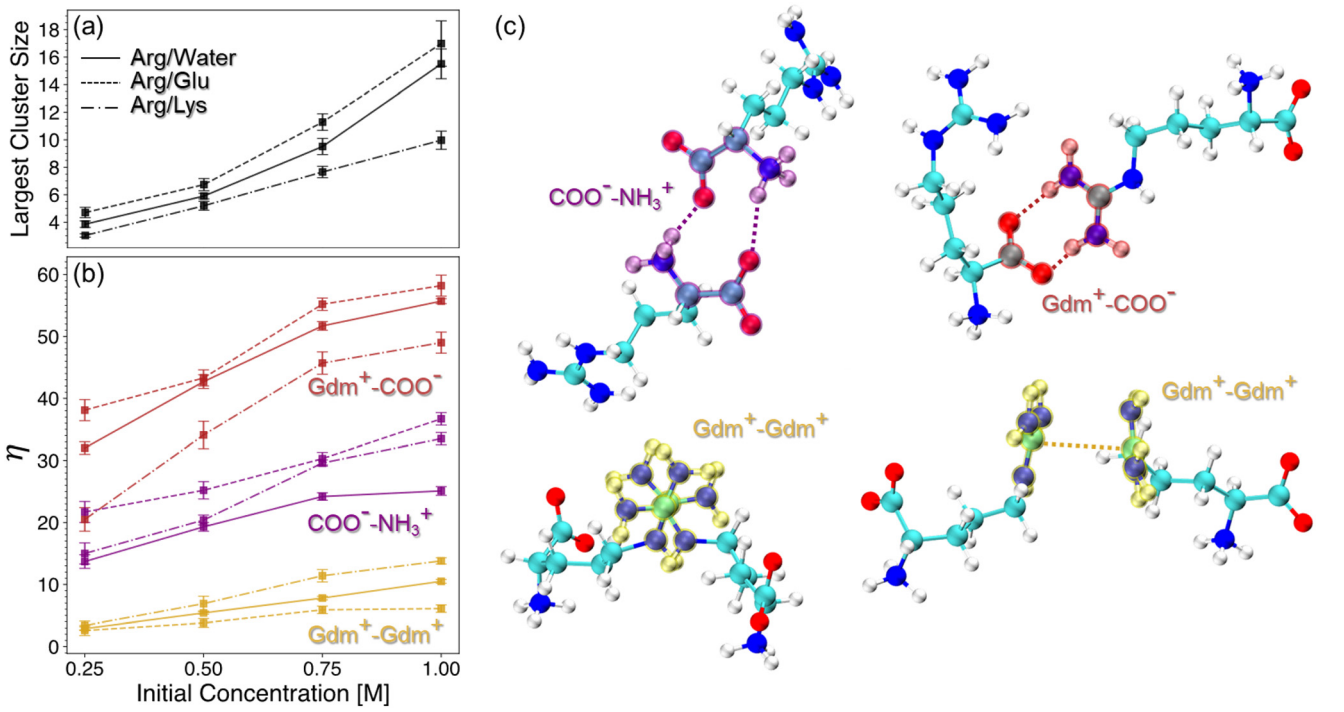

Fig. 8 Excipient clustering analysis. (a) Largest cluster size observed from excipient solutions as a function of concentration. (b) Contact efficiency metric (η) observed in excipient clusters for different solutions. (c) Representative configurations showing the three primary modes of excipient–excipient interactions. In (a) and (b), solid lines represent Arg/water solutions, dashed represents Arg/Glu, and dotted dashed lines represent Arg/Lys. In (b) and (c), different colors represent COO^-–NH_3^+ (purple), Gdm^+–COO^- (red), and Gdm^+–Gdm^+ (yellow) interaction types.

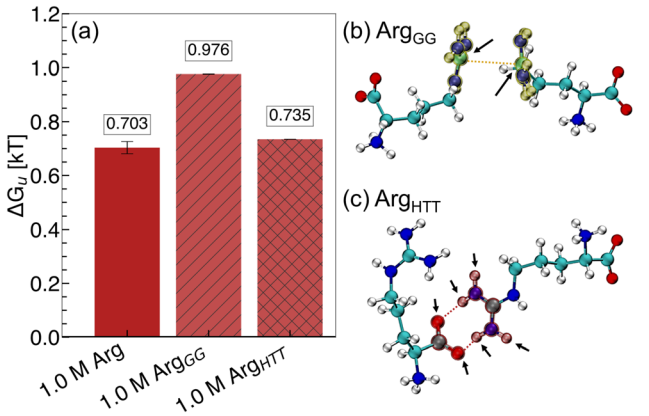

Fig. 9 Free energy of hydrophobic polymer unfolding in modified 1.0 M Arg/water solutions. (a) ΔG_u for unmodified Arg, increased Gdm^+–Gdm^+ interaction strength (Arg_{GG}), and increased Gdm^+–COO^- interaction strength (Arg_{HTT}). (b) Modified interactions in Arg_{GG}. (c) Modified interactions in Arg_{HTT}. In (b) and (c), arrows denote atoms with scaled interaction parameters.

To probe the importance of these interactions relevant to excipient clustering, we performed two additional REUS simulations of hydrophobic polymer folding with modified Arg–Arg interaction parameters (Fig. 9). To simulate increased Gdm^+–Gdm^+ pairing among Arg molecules (Arg_{GG}), we scaled the interaction strength between Gdm^+ carbon atoms by 150% (Fig. 9b). Similarly, to simulate increased Gdm^+–COO^- head-to-tail pairing among Arg molecules (Arg_{HTT}), the interaction strength between COO^- oxygen atoms and Gdm^+ hydrogen atoms was scaled by 150% (Fig. 9c). From these simulations, the free energy of polymer unfolding in Arg_{GG} solution becomes significantly less favorable relative to unmodified Arg solutions, while Arg_{HTT} results in only a small increase in folded state stability (Fig. 9a).

These results demonstrate the importance of the Gdm^+ sidechain of Arg in hydrophobic polymer unfolding. Gdm^+ is a known protein denaturant and has been shown to drive unfolding of an elongated hydrophobic polymer at high concentrations.[91] We have shown previously that direct interactions between the Gdm^+ sidechain of Arg and the hydrophobic polymer favors polymer folding at lower concentrations and are destabilizing at high concentrations.[40] Overall, our mechanistic explanation for Arg/Lys synergy involves a Lys-mediated increase in Gdm^+–Gdm^+ "stickiness" among Arg molecules. Upon addition of Lys, the increase in Gdm^+–Gdm^+ pairing among Arg molecules gives rise to the favorable change in $\Delta\Delta E_{pa}$ observed in Arg/Lys solutions. This is achieved by limiting the number of Gdm^+ interaction sites available to interact with the polymer, resulting in a relative depletion of Arg from the local polymer domain.

3.5.2 Explaining Arg/Glu synergy: the dynamics reducing hypothesis. While Arg/Lys synergy appears to be associated with changes in Gdm^+–Gdm^+ pairing among Arg molecules, we did not observe the same changes in excipient clustering in Arg/Glu solutions. Hence, to explain molecular-level changes linked to Arg/Glu synergy, we turned our attention to the behavior of water molecules in the local polymer environment.

We computed water reorientation dynamics in the local hydrophobic polymer domain for our excipient solutions (Fig. 10). The characteristic reorientation time for each solution was computed by fitting water dipole correlation functions to an exponential decay (Fig. S8†). With increasing excipient concentration, the reorientation time (τ) of local

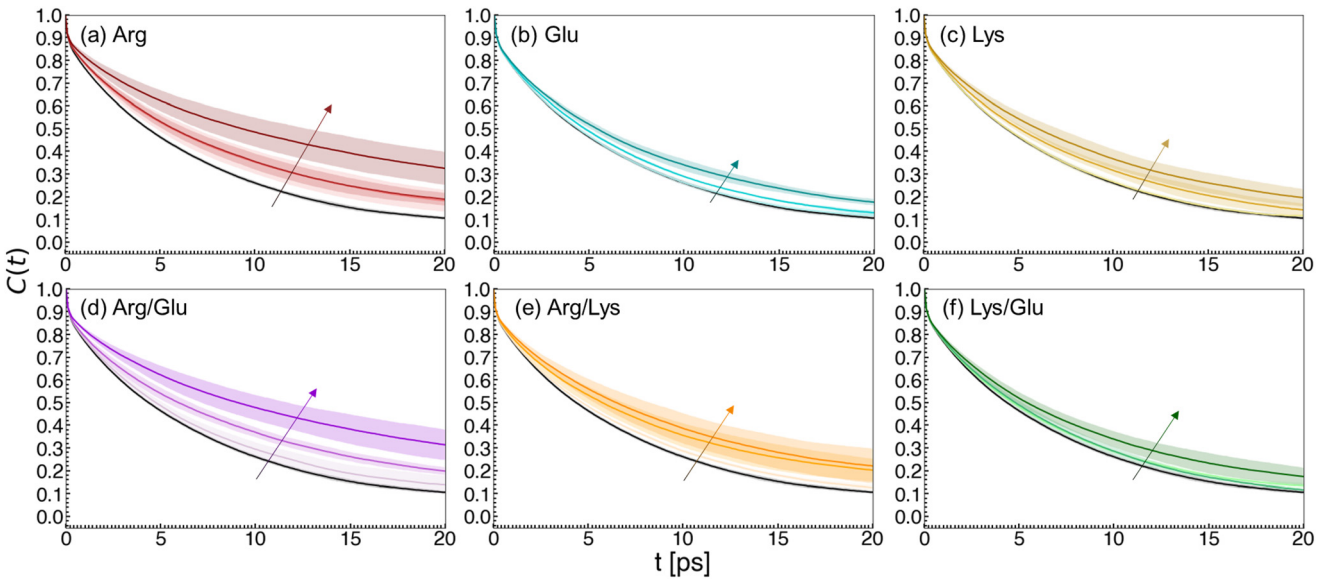

Fig. 10 Water reorientation dynamics in the local hydrophobic polymer domain. The time correlation function, $C(t)$, of instantaneous water dipole moments are plotted for (a) Arg/water, (b) Glu/water, (c) Lys/water, (d) Arg/Glu, (e) Arg/Lys, and (f) Lys/Glu solutions. Increasing excipient concentration is shown by increased shading, while values obtained in pure water are represented by black curves. Arrows are drawn to guide the change with concentration.

Table 1 Reorientation times (ps) of the instantaneous dipole vector of water molecules local to the hydrophobic polymer

Concentration (M)	Arg/water	Lys/water	Glu/water	Arg/Glu	Arg/Lys	Lys/Glu
0.0 M	6.54 (0.02)	—	—	—	—	—
0.25 M	8.52 (1.2)	6.46 (0.1)	6.49 (0.1)	7.07 (0.5)	7.24 (0.1)	6.9 (0.1)
0.5 M	8.64 (0.4)	7.85 (0.5)	7.17 (0.1)	8.86 (0.4)	8.56 (1.4)	7.17 (0.3)
1.0 M	**12.6 (1.0)**	9.29 (1.4)	8.4 (0.4)	**12.37 (0.8)**	8.81 (0.9)	8.48 (0.6)

water molecules was observed to increase, indicating a slowing of water dynamics (Table 1). This effect is most pronounced in Arg/water and Arg/Glu solutions.

Similar reductions in hydration shell dynamics have been associated with an increase in melting temperature of proteins. A recent study has proposed that stabilizing osmolytes slow down the dynamics of water, while denaturants accelerate water dynamics, inducing a pseudo-temperature change experienced by the protein.[137] Other studies have highlighted that some stabilizing excipients increase hydrogen bond relaxation time among water molecules and reduce rotational, translational, and tumbling motions of water.[126,138–142]

We hypothesize that the key consequence associated with this phenomenon is the formation of a rigid solvent network embedding the hydrophobic polymer in Arg/water and Arg/Glu solutions. In the case of Arg/Glu, Glu may provide an advantage relative to Arg/water alone due to a reduction of Gdm^+ sidechain accumulation in the local polymer domain, as reflected by Γ_{PA}. This results in the favorable change in $\Delta\Delta E_{pa}$, similar to Arg/Lys, while retaining the reduced water dynamics and stable local network associated with Arg solutions.

4 Conclusions

Excipient incorporation is a time-consuming and costly endeavor in the development of stable biologics. Excipients with high sensitivity to the solution environment, such as arginine, cause an additional layer of complexity to this step. In some cases, addition of co-excipients to formulations that include Arg has resulted in reversals[68] or synergistic[75] effects. Recently, we demonstrated that the peculiar placement of Arg at the edge of a mechanistic flip between indirect- and direct-dominated effects on hydrophobic interactions may be a key feature that allows tuning of the effect of Arg on stability.[40] Our findings here show that, not only is Arg a more effective stabilizer of hydrophobic interactions than its Lys or Glu counterparts, but the addition of these less effective excipients augments the effectiveness of Arg solution stability. For simplicity, we limited the scope of our solutions to 1 : 1 mole fractions of excipients in our binary mixtures. However, we acknowledge that there may be a limited range of mole fractions where excipient effects arise or even improve. Investigating the effect of varying the mole fractions of the binary components would be an appropriate direction for future studies.

We observed that the primary mechanism associated with Arg/Glu and Arg/Lys synergy is a substantial reduction in direct polymer–excipient interactions that oppose polymer folding at high Arg concentration. Through preferential interaction coefficient analysis, we further identified that Lys and Glu are both effective at reducing the relative accumulation of Arg molecules in the local polymer domain, providing a molecular explanation for the favorable change in $\Delta\Delta E_{pa}$.

Analysis of the solvent network embedding the hydrophobic polymer provides an explanation for how excipients alter the local solvent environment. We found that Arg increases connectivity among water molecules, integrates favorably into the local environment, and increases the stability of the network by delaying the onset of simulated graph fragmentation. These features are more pronounced in Arg solutions than in Lys, Glu, or Lys/Glu solutions. Importantly, we identified these same features in Arg/Lys and Arg/Glu solutions, indicating that stabilizing co-excipients preserve the network effects of Arg.

Finally, we established two hypotheses for Arg/Lys and Arg/Glu synergy. In the case of Arg/Lys, there is an increase in Gdm^+–Gdm^+ pairing among Arg molecules, reducing the number of available Gdm^+ sidechains that drive polymer unfolding at high concentrations. From simulations of increased Gdm^+–Gdm^+ interaction strength between Arg molecules, we found this change to be sufficient for stabilizing polymer folding. In the case of Arg/Glu, we did not find increased Gdm^+–COO^- pairing in solution was sufficient to drive co-excipient synergy. However, we observed a reduction in the dynamics of water molecules local to the hydrophobic polymer in these solutions. Similar reductions in local water dynamics have been linked to increased melting temperature of proteins in the presence of stabilizing osmolytes.[126,138–142]

In this study, we demonstrated that changes in excipient composition alter hydrophobic interactions, the dominant force associated with several biologically-important processes including protein folding and self-assembly. As it pertains to formulations, this is an important factor in preventing protein denaturation and aggregation. Due to its placement on the edge of a mechanistic flip, formulations containing Arg as an excipient may be improved by shifting the balance of direct- and indirect-mediated effects. To this end, we increased the relative stability of hydrophobic polymer folding by reducing destabilizing direct effects *via* co-excipient addition of either Lys or Glu. Overall, these results highlight the investigation of molecular-level insights of

excipient mechanisms as an important endeavor in the rational design of stable biologics. In future studies, the hydrophobic polymer model can be built upon by studying systems with added complexity such as polyelectrolytes, block copolymers, and miniproteins.

Data availability

Data for this article, including simulation parameter files and analysis scripts, are available at **https://github.com/SAMPEL-Group/Hydrophobic-Polymer-Binary-Excipients**.

Author contributions

JWPZ: investigation – computational, validation, formal analysis, visualization, writing – original draft, writing – review and editing; PM: investigation – computational, validation, writing – review and editing; CLH: conceptualization, funding acquisition, resources, writing – review and editing; SLP: conceptualization, funding acquisition, resources, writing – review and editing; SS: conceptualization, methodology, validation, supervision, project administration, funding acquisition, resources, writing – review and editing.

Conflicts of interest

There are no conflicts to declare.

Acknowledgements

This material is based upon work supported by the National Science Foundation under DMREF Grant No. 2118788, 2118693, and 2118638. Computational resources were provided by the Minnesota Supercomputing Institute at the University of Minnesota – Twin Cities.

References

1 M. A. Strassburg, *Am. J. Infect. Control*, 1982, **10**, 53–59.
2 W.-W. Zhang, L. Li, D. Li, J. Liu, X. Li, W. Li, X. Xu, M. J. Zhang, L. A. Chandler, H. Lin, A. Hu, W. Xu and D. M.-K. Lam, *Hum. Gene Ther.*, 2018, **29**, 160–179.
3 P. L. Privalov, *Crit. Rev. Biochem. Mol. Biol.*, 1990, **25**, 281–306.
4 K. Heremans, *Annu. Rev. Biophys. Bioeng.*, 1982, **11**, 1–21.
5 S. Sarupria, T. Ghosh, A. E. García and S. Garde, *Proteins: Struct., Funct., Bioinf.*, 2010, **78**(7), 1641–1651.
6 W. Kauzmann, *Advances in Protein Chemistry*, Elsevier, 1959, vol. 14, pp. 1–63.
7 H. S. Frank and M. W. Evans, *J. Chem. Phys.*, 1945, **13**, 507–532.
8 L. K. Christensen, *C. R. Trav. Lab. Carlsberg, Ser. Chim.*, 1952, **28**, 37–69.
9 G. Hummer, S. Garde, A. E. García, M. E. Paulaitis and L. R. Pratt, *Proc. Natl. Acad. Sci. U. S. A.*, 1998, **95**, 1552–1555.
10 T. Ghosh, A. E. García and S. Garde, *J. Am. Chem. Soc.*, 2001, **123**, 10997–11003.
11 Y. Le Basle, P. Chennell, N. Tokhadze, A. Astier and V. Sautou, *J. Pharm. Sci.*, 2020, **109**, 169–190.
12 J.-R. Authelin, M. A. Rodrigues, S. Tchessalov, S. K. Singh, T. McCoy, S. Wang and E. Shalaev, *J. Pharm. Sci.*, 2020, **109**, 44–61.
13 D. J. A. Crommelin, A. Hawe and W. Jiskoot, *Formulation of Biologics Including Biopharmaceutical Considerations*, Springer International Publishing, Cham, 2024, pp. 95–117.
14 B. R. Clarkson, A. Schön and E. Freire, *Drug Discovery Today*, 2016, **21**, 342–347.
15 A. Mazzeo and P. Carpenter, *Handbook of Stability Testing in Pharmaceutical Development*, Springer New York, New York, NY, 2009, pp. 353–369.
16 C. M. Hanson, A. M. George, A. Sawadogo and B. Schreiber, *Vaccine*, 2017, **35**, 2127–2133.
17 Y. B. Yu, K. T. Briggs, M. B. Taraban, R. G. Brinson and J. P. Marino, *Pharm. Res.*, 2021, **38**, 3–7.
18 D. J. Crommelin, T. J. Anchordoquy, D. B. Volkin, W. Jiskoot and E. Mastrobattista, *J. Pharm. Sci.*, 2021, **110**, 997–1001.
19 A. Thielmann, M.-T. Puth and B. Weltermann, *PLoS One*, 2019, **14**, e0225764.
20 A. Thielmann, M.-T. Puth and B. Weltermann, *Vaccine*, 2020, **38**, 7551–7557.
21 T. J. Kamerzell, R. Esfandiary, S. B. Joshi, C. R. Middaugh and D. B. Volkin, *Adv. Drug Delivery Rev.*, 2011, **63**, 1118–1159.
22 T. Arakawa, K. Tsumoto, Y. Kita, B. Chang and D. Ejima, *Amino Acids*, 2007, **33**, 587–605.
23 A. Bongioanni, M. S. Bueno, B. A. Mezzano, M. R. Longhi and C. Garnero, *Int. J. Pharm.*, 2022, **613**, 121375.
24 S. H. Jeong, *Arch. Pharmacal Res.*, 2012, **35**, 1871–1886.
25 W. Wang, *Int. J. Pharm.*, 2005, **289**, 1–30.
26 S. Y. Patro, E. Freund and B. S. Chang, *Biotechnology Annual Review*, Elsevier, 2002, vol. 8, pp. 55–84.
27 Y. Ionova and L. Wilson, *PLoS One*, 2020, **15**, e0235076.
28 M. A. Capelle, R. Gurny and T. Arvinte, *Eur. J. Pharm. Biopharm.*, 2007, **65**, 131–148.
29 M. Zidar, G. Posnjak, I. Muševič, M. Ravnik and D. Kuzman, *Pharm. Res.*, 2020, **37**, 27.
30 S. J. Shire, *Curr. Opin. Biotechnol.*, 2009, **20**, 708–714.
31 V. S. Dave, S. D. Saoji, N. A. Raut and R. V. Haware, *J. Pharm. Sci.*, 2015, **104**, 906–915.
32 Y. B. Yu, M. B. Taraban, K. T. Briggs, R. G. Brinson and J. P. Marino, *Pharm. Res.*, 2021, **38**, 2179–2184.
33 D. P. Elder, M. Kuentz and R. Holm, *Eur. J. Pharm. Sci.*, 2016, **87**, 88–99.
34 P. R. ten Wolde and D. Chandler, *Proc. Natl. Acad. Sci. U. S. A.*, 2002, **99**, 6539–6543.
35 R. Zangi, R. Zhou and B. J. Berne, *J. Am. Chem. Soc.*, 2009, **131**, 1535–1541.
36 D. Nayar and N. F. A. van der Vegt, *J. Phys. Chem. B*, 2018, **122**, 3587–3595.
37 J. Mondal, G. Stirnemann and B. J. Berne, *J. Phys. Chem. B*, 2013, **117**, 8723–8732.
38 M. V. Athawale, S. Sarupria and S. Garde, *J. Phys. Chem. B*, 2008, **112**, 5661–5670.

39 S. N. Jamadagni, R. Godawat and S. Garde, *Langmuir*, 2009, **25**, 13092–13099.
40 J. W. P. Zajac, P. Muralikrishnan, I. Tohidian, X. Zeng, C. L. Heldt, S. L. Perry and S. Sarupria, *arXiv*, 2024, preprint, arXiv:2403.11305 [cond-mat], DOI: **10.48550/arXiv.2403.11305**.
41 C. Tanford, *J. Am. Chem. Soc.*, 1962, **84**, 4240–4247.
42 C. Tanford, *Science*, 1978, **200**, 1012–1018.
43 K. A. Dill, *Biochemistry*, 1990, **29**, 7133–7155.
44 H. J. Savage, C. J. Elliott, C. M. Freeman and J. L. Finney, *J. Chem. Soc., Faraday Trans.*, 1993, **89**, 2609.
45 G. Hummer, S. Garde, A. Garcia and L. Pratt, *Chem. Phys.*, 2000, **258**, 349–370.
46 L. R. Pratt and A. Pohorille, *Chem. Rev.*, 2002, **102**, 2671–2692.
47 A. Ben-Naim, *Hydrophobic interactions*, Plenum Press, New York, 2005.
48 D. Chandler, *Nature*, 2005, **437**, 640–647.
49 A. Wallqvist, D. G. Covell and D. Thirumalai, *J. Am. Chem. Soc.*, 1998, **120**, 427–428.
50 M. Ikeguchi, S. Nakamura and K. Shimizu, *J. Am. Chem. Soc.*, 2001, **123**, 677–682.
51 T. Ghosh, A. Kalra and S. Garde, *J. Phys. Chem. B*, 2005, **109**, 642–651.
52 N. F. A. Van Der Vegt, M.-E. Lee, D. Trzesniak and W. F. Van Gunsteren, *J. Phys. Chem. B*, 2006, **110**, 12852–12855.
53 M.-E. Lee and N. F. A. Van Der Vegt, *J. Am. Chem. Soc.*, 2006, **128**, 4948–4949.
54 T. A. Shpiruk and M. Khajehpour, *Phys. Chem. Chem. Phys.*, 2013, **15**, 213–222.
55 M. V. Athawale, J. S. Dordick and S. Garde, *Biophys. J.*, 2005, **89**, 858–866.
56 S. Paul and G. N. Patey, *J. Phys. Chem. B*, 2008, **112**, 11106–11111.
57 R. D. Macdonald and M. Khajehpour, *Biophys. Chem.*, 2013, **184**, 101–107.
58 P. Ganguly, N. F. A. Van Der Vegt and J.-E. Shea, *J. Phys. Chem. Lett.*, 2016, **7**, 3052–3059.
59 Z. Su, G. Ravindhran and C. L. Dias, *J. Phys. Chem. B*, 2018, **122**, 5557–5566.
60 A. Folberth, S. Bharadwaj and N. F. A. Van Der Vegt, *Phys. Chem. Chem. Phys.*, 2022, **24**, 2080–2087.
61 P. Ganguly, D. Bubák, J. Polák, P. Fagan, M. Dračínská, N. F. A. Van Der Vegt, J. Heyda and J.-E. Shea, *J. Phys. Chem. Lett.*, 2022, **13**, 7980–7986.
62 K. Tsumoto, M. Umetsu, I. Kumagai, D. Ejima, J. Philo and T. Arakawa, *Biotechnol. Prog.*, 2004, **20**, 1301–1308.
63 K. Tsumoto, D. Ejima, Y. Kita and T. Arakawa, *Protein Pept. Lett.*, 2005, **12**, 613–619.
64 P. Stärtzel, *J. Pharm. Sci.*, 2018, **107**, 960–967.
65 J. Hamborsky, A. Kroger and C. Wolfe, *Epidemiology and prevention of vaccine-preventable diseases*, Centers for Disease Control and Prevention, Atlanta, GA, 13th edn, 2015.
66 M. J. Mistilis, J. C. Joyce, E. S. Esser, I. Skountzou, R. W. Compans, A. S. Bommarius and M. R. Prausnitz, *Drug Delivery Transl. Res.*, 2017, **7**, 195–205.
67 Q. Xie, T. Guo, J. Lu and H.-M. Zhou, *Int. J. Biochem. Cell Biol.*, 2004, **36**, 296–306.
68 B. Anumalla and N. P. Prabhu, *Appl. Biochem. Biotechnol.*, 2019, **189**, 541–555.
69 T. Arakawa and N. K. Maluf, *Int. J. Biol. Macromol.*, 2018, **107**, 1692–1696.
70 E. Smirnova, I. Safenkova, B. Stein-Margolina, V. Shubin and B. Gurvits, *Amino Acids*, 2013, **45**, 845–855.
71 D. Shah, A. R. Shaikh, X. Peng and R. Rajagopalan, *Biotechnol. Prog.*, 2011, **27**, 513–520.
72 T. B. Eronina, N. A. Chebotareva, N. N. Sluchanko, V. V. Mikhaylova, V. F. Makeeva, S. G. Roman, S. Y. Kleymenov and B. I. Kurganov, *Int. J. Biol. Macromol.*, 2014, **68**, 225–232.
73 C. Meingast and C. L. Heldt, *Biotechnol. Prog.*, 2020, **36**, e2931.
74 C. L. Meingast, P. U. Joshi, D. G. Turpeinen, X. Xu, M. Holstein, H. Feroz, S. Ranjan, S. Ghose, Z. J. Li and C. L. Heldt, *Biotechnol. J.*, 2021, **16**, 2000342.
75 D. Shukla and B. L. Trout, *J. Phys. Chem. B*, 2011, **115**, 11831–11839.
76 Y. Sugita, A. Kitao and Y. Okamoto, *J. Chem. Phys.*, 2000, **113**, 6042–6051.
77 J. L. F. Abascal and C. Vega, *J. Chem. Phys.*, 2005, **123**, 234505.
78 B. R. Brooks, R. E. Bruccoleri, B. D. Olafson, D. J. States, S. Swaminathan and M. Karplus, *J. Comput. Chem.*, 1983, **4**, year.
79 B. R. Brooks, C. L. Brooks, A. D. Mackerell, L. Nilsson, R. J. Petrella, B. Roux, Y. Won, G. Archontis, C. Bartels, S. Boresch, A. Caflisch, L. Caves, Q. Cui, A. R. Dinner, M. Feig, S. Fischer, J. Gao, M. Hodoscek, W. Im, K. Kuczera, T. Lazaridis, J. Ma, V. Ovchinnikov, E. Paci, R. W. Pastor, C. B. Post, J. Z. Pu, M. Schaefer, B. Tidor, R. M. Venable, H. L. Woodcock, X. Wu, W. Yang, D. M. York and M. Karplus, *J. Comput. Chem.*, 2009, **30**, 1545–1614.
80 G. Bussi, D. Donadio and M. Parrinello, *J. Chem. Phys.*, 2007, **126**, 014101.
81 H. J. Berendsen, J. P. Postma, W. F. van Gunsteren, A. DiNola and J. R. Haak, *J. Chem. Phys.*, 1984, **81**, 3684–3690.
82 D. J. Evans and B. L. Holian, *J. Chem. Phys.*, 1985, **83**, 4069–4074.
83 M. Parrinello and A. Rahman, *J. Appl. Phys.*, 1981, **52**, 7182–7190.
84 H. A. Lorentz, *Ann. Phys.*, 1881, **248**, 127–136.
85 D. Berthelot, *Compt. Rendus*, 1898, **126**, 1703–1855.
86 E. Lindahl, M. J. Abraham, B. Hess and D. van der Spoel, *Gromacs 2021.4 source code*, 2021, **https://zenodo.org/record/5636567**.
87 T. P. Consortium, *Nat. Methods*, 2019, **16**, 670–673.
88 G. A. Tribello, M. Bonomi, D. Branduardi, C. Camilloni and G. Bussi, *Comput. Phys. Commun.*, 2014, **185**, 604–613.
89 F. Zhu and G. Hummer, *J. Comput. Chem.*, 2011, **33**, 453–465.
90 M. V. Athawale, G. Goel, T. Ghosh, T. M. Truskett and S. Garde, *Proc. Natl. Acad. Sci. U. S. A.*, 2007, **104**, 733–738.
91 R. Godawat, S. N. Jamadagni and S. Garde, *J. Phys. Chem. B*, 2010, **114**, 2246–2254.

92 N. F. A. van der Vegt and D. Nayar, *J. Phys. Chem. B*, 2017, **121**, 9986–9998.
93 S. Dasetty and S. Sarupria, *J. Phys. Chem. B*, 2021, **125**, 2644–2657.
94 L. R. Pratt and D. Chandler, *J. Chem. Phys.*, 1977, **67**, 3683–3704.
95 K. Lum, D. Chandler and J. D. Weeks, *J. Phys. Chem. B*, 1999, **103**, 4570–4577.
96 P. R. T. Wolde, *J. Phys.: Condens. Matter*, 2002, **14**, 9445–9460.
97 D. M. Huang and D. Chandler, *J. Phys. Chem. B*, 2002, **106**, 2047–2053.
98 S. Garde, A. E. Garcia, L. R. Pratt and G. Hummer, *Biophys. Chem.*, 1999, **78**, 21–32.
99 D. Ben-Amotz, *Annu. Rev. Phys. Chem.*, 2016, **67**, 617–638.
100 G. Scatchard, *J. Am. Chem. Soc.*, 1946, **68**, 2315–2319.
101 E. F. Casassa and H. Eisenberg, *Adv. Protein Chem.*, 1964, **19**, 287–395.
102 J. A. Schellman, *Biopolymers*, 1987, **26**, 549–559.
103 H. Inoue and S. N. Timasheff, *Biopolymers*, 1972, **11**, 737–743.
104 M. Record and C. Anderson, *Biophys. J.*, 1995, **68**, 786–794.
105 D. Shukla, C. Shinde and B. L. Trout, *J. Phys. Chem. B*, 2009, **113**, 12546–12554.
106 J. Wyman, *Advances in Protein Chemistry*, Elsevier, 1964, vol. 19, pp. 223–286.
107 S. N. Timasheff, *Proc. Natl. Acad. Sci. U. S. A.*, 2002, **99**, 9721–9726.
108 D. Shukla, C. P. Schneider and B. L. Trout, *Adv. Drug Delivery Rev.*, 2011, **63**, 1074–1085.
109 D. R. Canchi and A. E. García, *Annu. Rev. Phys. Chem.*, 2013, **64**, 273–293.
110 J. Mondal, D. Halverson, I. T. S. Li, G. Stirnemann, G. C. Walker and B. J. Berne, *Proc. Natl. Acad. Sci. U. S. A.*, 2015, **112**, 9270–9275.
111 M. Mukherjee and J. Mondal, *J. Phys. Chem. B*, 2020, **124**, 6565–6574.
112 U. Das, G. Hariprasad, A. S. Ethayathulla, P. Manral, T. K. Das, S. Pasha, A. Mann, M. Ganguli, A. K. Verma, R. Bhat, S. K. Chandrayan, S. Ahmed, S. Sharma, P. Kaur, T. P. Singh and A. Srinivasan, *PLoS One*, 2007, **2**, e1176.
113 C. P. Schneider and B. L. Trout, *J. Phys. Chem. B*, 2009, **113**, 2050–2058.
114 D. Shukla and B. L. Trout, *J. Phys. Chem. B*, 2010, **114**, 13426–13438.
115 C. P. Schneider, D. Shukla and B. L. Trout, *J. Phys. Chem. B*, 2011, **115**, 7447–7458.
116 V. Vagenende, A. X. Han, M. Mueller and B. L. Trout, *ACS Chem. Biol.*, 2013, **8**, 416–422.
117 S. Santra, S. Dhurua and M. Jana, *J. Chem. Phys.*, 2021, **154**, 084901.
118 S. Santra and M. Jana, *J. Phys. Chem. B*, 2022, **126**, 1462–1476.
119 A. A. Hagberg, D. A. Schult and P. J. Swart, Exploring network structure, dynamics, and function using NetworkX, in *Proceedings of the 7th Python in Science Conference (SciPy2008)*, 2008, pp. 11–15.
120 S. Wasserman and K. Faust, *Social Network Analysis: Methods and Applications*, Cambridge University Press, 1st edn, 1994.
121 L. C. Freeman, *Soc. Netw.*, 1978, **1**, 215–239.
122 U. Brandes, *J. Math. Sociol.*, 2001, **25**, 163–177.
123 U. Brandes, *Soc. Netw.*, 2008, **30**, 136–145.
124 K. Schrenk, M. Hilário, V. Sidoravicius, N. Araújo, H. Herrmann, M. Thielmann and A. Teixeira, *Phys. Rev. Lett.*, 2016, **116**, 055701.
125 H. Liu, S. Xiang, H. Zhu and L. Li, *Molecules*, 2021, **26**, 5403.
126 A. Diaz and V. Ramakrishnan, *Comput. Biol. Chem.*, 2023, **105**, 107883.
127 L. McInnes, J. Healy and S. Astels, *J. Open Source Softw.*, 2017, **2**, 205.
128 M. Miotto, N. Warner, G. Ruocco, G. G. Tartaglia, O. A. Scherman and E. Milanetti, *arXiv*, 2023, preprint, arXiv:2305.05038v1 [q-bio.BM], DOI: **10.48550/arXiv.2305.05038**.
129 S. Sundar, A. A. Sandilya and M. H. Priya, *J. Chem. Inf. Model.*, 2021, **61**, 3927–3944.
130 N. E. Brunk, L. S. Lee, J. A. Glazier, W. Butske and A. Zlotnick, *Phys. Biol.*, 2018, **15**, 056005.
131 N. E. Brunk and R. Twarock, *ACS Nano*, 2021, **15**, 12988–12995.
132 Y. Rubner and C. Tomasi, *The Earth Mover's Distance*, Springer US, Boston, MA, 2001, pp. 13–28.
133 P. Gund, *J. Chem. Educ.*, 1972, **49**, 100.
134 P. E. Mason, G. W. Neilson, C. E. Dempsey, A. C. Barnes and J. M. Cruickshank, *Proc. Natl. Acad. Sci. U. S. A.*, 2003, **100**, 4557–4561.
135 O. Shih, A. H. England, G. C. Dallinger, J. W. Smith, K. C. Duffey, R. C. Cohen, D. Prendergast and R. J. Saykally, *J. Chem. Phys.*, 2013, **139**, 035104.
136 M. Vazdar, J. Heyda, P. E. Mason, G. Tesei, C. Allolio, M. Lund and P. Jungwirth, *Acc. Chem. Res.*, 2018, **51**, 1455–1464.
137 M. Hishida, R. Anjum, T. Anada, D. Murakami and M. Tanaka, *J. Phys. Chem. B*, 2022, **126**, 2466–2475.
138 G. S. Jas, E. C. Rentchler, A. M. Słowicka, J. R. Hermansen, C. K. Johnson, C. R. Middaugh and K. Kuczera, *J. Phys. Chem. B*, 2016, **120**, 3089–3099.
139 G. Saladino, M. Marenchino, S. Pieraccini, R. Campos-Olivas, M. Sironi and F. L. Gervasio, *J. Chem. Theory Comput.*, 2011, **7**, 3846–3852.
140 I. Jahan and S. M. Nayeem, *RSC Adv.*, 2020, **10**, 27598–27614.
141 J. Zeman, C. Holm and J. Smiatek, *J. Chem. Eng. Data*, 2020, **65**, 1197–1210.
142 R. Gazi, S. Maity and M. Jana, *ACS Omega*, 2023, **8**, 2832–2843.